Mechanised Harvesting of Standing Trees Using Contact Ultrasonic Testing and Machine Learning

Mohsen Mousavi[a], Mohammad Sadegh Taskhiri[b], Amir H Gandomi *[a]

[a] *Faculty of Engineering and IT, University of Technology Sydney, Ultimo, NSW 2007, Australia*
[b] *Waste Economics Institute of Sustainable Industries & Liveable Cities, Victoria University, VIC 8009, Australia*

Abstract

The problem of hole-defect detection in standing trees is solved. To this end, the contact–ultrasonic device (Pundit PL-200) was employed to collect ultrasonic signals from testing some wood specimens both in the lab and some sites in Australia. The collected ultrasonic signals were then processed through the Variational Mode Decomposition algorithm to derive some features. In order to solve the classification problem more efficiently, the obtained characteristics were then analyzed through PCA to determine the most compelling features. Several machine learning algorithms and a one-dimensional convolutional neural network (1D-CNN) were employed to solve a set of classification problems based on data collected from (1) specimens with artificial defects in the lab and (2) billets with natural defects selected from trees harvested in sites of two states of WA and NSW, Australia. The results demonstrate the effectiveness of the proposed method for classifying wood materials based on their health state, where the accuracy result of 100% in the lab and at least 92.4% in the fields were achieved. The Fine Gaussian SVM was found to perform best on data collected from specimens in the lab and fields. It was also shown that 1D-CNN results were more reliable for solving the classification problem of standing trees in the fields.

Keywords: `Contact-ultrasonic testing, Machine learning, One dimensional CNN, Feature engineering, Variational mode decomposition`

Email address: `gandomi@uts.edu.au` (Amir H Gandomi *)

1. Introduction

Modern Detection and Diagnosis (FDD) systems involve several steps, including (1) system knowledge representation, (2) data-acquisition and signal processing, (3) fault classification, and (4) maintenance-related decision making [1]. Conventional decay assessment of trees involves visual inspection to detect any external evidence that corresponds to the structural deficiency. Some of such evidence includes wounds at the tree's self-pruned branches, which can occur when the trees are not pruned in time and, therefore, undergo a self-pruning process. Some invasive methods are used for decay detection in standing trees, such as decay detecting drill [2]. As such, a noninvasive sensing technology for detecting wood defects in standing trees is yet to be developed.

Monitoring wood quality is of great interest to the mechanised harvesting industry [3]. For instance, it is known that the existence of knot clusters can affect the mechanical properties of wood products [4]. Wood material assessment favours the extensive development of new nondestructive techniques developed over the past decades. Such techniques usually comprise two elements: a sensing technology for collecting data of a wooden specimen and a data analysis algorithm that can interpret such data by deriving some features that can characterise the health state of the wood. Some of such sensing technologies include ultrasonics [5], thermography [6], and radiography [7]. Ultrasonic testing has been widely used for quality assessment of wood materials [8] due to the following reasons: (1) it is a less invasive and less expensive technique compared to other methods, and (2) it is susceptible to the existence of defects in wood materials [9]. Therefore, they have been used in several research for quality assessment of wooden sections [10, 11, 12, 13, 14, 15]. For instance, the capability of ultrasonic techniques for evaluating of mechanical properties of wood with artificial defects has been demonstrated in several studies [11, 16, 17, 18]. Ultrasonic tomography was also demonstrated as an effective method for detecting defects in standing trees [19], where it was shown that the velocity of the ultrasonic waves was correlated with the ratio of the hole-to-disc area. Another study found that the attenuation of the ultrasonic wave velocity and increased damping could be correlated with the presence of a defect in standing trees [20]. However, it was also learned that both ultrasound velocity and damping were sensitive to the diameter at the breast height (DBH) of the studied tree. A binary logistic regression was developed to explore the possibility of using ultrasound velocity and damping to predict internal defects' presence in stating trees [20]. The obtained accuracy using the velocity and damping were respectively 0.72 and 0.76 in European beech and 0.83 and 0.82 in Norway spruce spices. Studying the time of flight of the ultrasonic waves travelling across the wood sections has also been demonstrated to be effective for evaluating defects in standing trees. In another study, a time-frequency signal processing algorithm was coupled with the ultrasound's time of flight to evaluate the wood quality of standing trees [21].

There are generally two types of ultrasonic devices based on how they are used to test specimens. This includes non-contact and contact devices. There are several types of non-contact–ultrasonics such as laser ultrasonics (LU) [22], electromagnet ultrasonics (EU) [23], and air-coupled ultrasonics (ACU) [24, 25, 26, 27]. Non-contact–ultrasonic techniques are widely used for NDT of different materials, though some limitations of such techniques have been reported in the literature. For example, EU devices are limited to conductive materials; LU devices are costly; ACU devices can only perform well in low-density materials [26]. Nonetheless, ACU signals can be of poor quality, further demanding more advanced signal processing algorithms for signal processing of the test results [25]. contact–ultrasonics can also suffer from several challenges. These devices include a transmitter and a receiver to perform the ultrasonic test on a specimen. However, a couplant gel must be applied to the surface of the sample at both receiver and transmitter sides to overcome the impedance difference between the air and the tested material. This will further ensure good transmissibility of the ultrasonic wave into the material by filling the gap between the transducer/receiver and the surface of the specimen. However, uncertainty always involves the amount of gel applied to the surface of the specimen for testing. Moreover, applying excessive pressure to the transducer/receiver by hand can squeeze some gel out of the gap, further compromising the quality of the test results. Moreover, any misalignment or vibration of the transducer/receiver can adversely affect the quality of measurements.

This study explores the possibility of using contact–ultrasonics to mechanize standing tree harvesting. Generally, it is important to prune trees in time for self-pruning. The trees that have undergone self-pruning are usually found to be knotty and inappropriate for sawlogs [28]. Therefore, it is essential to hunt such trees down in the field prior to cultivation. Two different experiments, one in the lab and one in the field, were conducted in this study to explore the possibility of using contact–ultrasonic testing to classify wooden specimens into two categories: defective and healthy. Regarding the lab trial, two types of wood specimens, Merbau and Pine, were studied. In order to synthesize hole-defect in the specimens, two types of hole of different sizes were drilled into the models; one small and one large. The samples were classified as defective regardless of the size of the hole defects to make the experiment more compatible with the test conducted in the field. Regarding the tests performed in the field, first, some billets were cut from the cultivated trees in different sites of Collie (WA) and Coffs harbour (NSW), Australia. Other types of wood were studied in these sites, including Eucalyptus Marginata (Jarrah), Eucalyptus Pilularis (Blackbutt) and Eucalyptus Punctata (Grey gum). The proposed strategy uses the variational mode decomposition (VMD) algorithm to derive some features from the ultrasonic test results conducted on the studied specimens. Next, machine learning and deep learning models were trained to solve the classification problem of the tested samples into two categories healthy and defective. This study presents several novelties as listed below:

1. First, the possibility of using VMD as a signal decomposition algorithm for feature extraction out of ultrasonic test results is demonstrated by introducing some useful features.
2. Since the number of features extracted from the VMD can be numerous; a procedure is proposed to select the most appropriate features for solving the classification problems of this paper. Moreover, it was demonstrated that there is quite an overlap between the selected features from the lab and

the field's test results.

3. The proposed strategy is further successfully tested on some standing trees in the field by employing trained machine learning and deep learning algorithms.

2. Methodology

2.1. Feature extraction using VMD

Each ultrasonic signal $S(t)$ was first shifted by its mean value and then scaled by the difference between its maximum and minimum values as follows:

$$\overline{\mathbf{S}}(t) = \frac{\mathbf{S}(t) - \mu}{\max(\mathbf{S}(t)) - \min(\mathbf{S}(t))}. \tag{1}$$

where $\overline{S}(t)$ is the normalised version of $S(t)$. The normalised signals were then low-pass filtered with a cutoff frequency of 300 kHz [29]. The VMD algorithm was employed to derive some features from the normalised and low-passed filtered ultrasonic signals. Hence, a brief background of the VMD theory is presented here to keep the paper self-contained.

VMD solves a variational optimisation problem to decompose a nonlinear/non-stationary signal into its constructive modes termed Intrinsic Mode Functions (IMFs). Each IMF is narrow-band and, therefore, can represent only one mode of oscillation of the signal. The general form of the k^{th} IMF is as follows:

$$\mathbf{u}_k(t) = \mathbf{A}_k(t)\ \cos(\phi_k(t)), \tag{2}$$

where $\mathbf{u}_k(t)$ is the k^{th} IMF with $\mathbf{A}_k(t)$ and $\phi_k(t)$ being its instantaneous amplitude and phase, respectively. The Instantaneous Frequency (IF) of each IMF is obtained as $\omega(t) = \frac{\partial \phi(t)}{\partial t}$. Alternatively, once an IMF is identified, the IF signal can be obtained through Gabor's analytical signal defined as follows [30]:

$$\mathbf{u}_a(t) = \mathbf{u}(t) + j\hat{\mathbf{u}}(t), \tag{3}$$

where $\mathbf{u}_a(t)$ is the Gabor's analytical signal, j is the imaginary unit, and $\hat{\mathbf{u}}(t)$ is the Hilbert transform [31] of the given IMF signal $\mathbf{u}(t)$. As such, the instantaneous frequency of the IMF is obtained as follows:

$$\omega(t) = \frac{\mathrm{d}}{\mathrm{d}t}\left(\tan^{-1}\left(\frac{\mathbf{u}\hat{(t)}}{\mathbf{u}(t)}\right)\right), \tag{4}$$

The following procedures are followed to construct the variational optimisation problem of the VMD:

Step (1): First the unilateral Hilbert transform of the k^{th} IMF is obtained as $\left(\delta(t) + \frac{j}{\pi t}\right) * \mathbf{u}_k(t)$, where δ, j, and $*$ denote the Dirac distribution, the imaginary unit, and the convolution operator, respectively.

Step (2): A center frequency ω_k is assumed for the k^{th} IMF and the obtained Hilbert spectrum from the step (1) is shifted to the baseband as $\left[\left(\delta(t) + \frac{j}{\pi t}\right) * \mathbf{u}_k(t)\right] \times e^{-j\omega_k t}$.

Step (3): Then, the squared L^2 norm of the gradient of the shifted spectrum from the step (2) is calculated as $\left\| \partial_t \left[\left(\delta(t) + \frac{j}{\pi t}\right) * \mathbf{u}_k(t)\right] \times e^{-j\omega_k t} \right\|^2$.

Table 1: VMD PARAMETERS.

Parameters	Description	Specified values
p	Number of IMFs	3
α	Denoising factor	N.A.
τ	Time interval	0.1
ϵ	Convergence threshold	10^{-5}
init	Center frequency initialiser	0
DC	Boolean parameter	0

Step (4): Finally, the L^2 norm of the gradients is summed over all IMFs to construct the conditional optimisation problem of the VMD, on $\mathbf{u}_k$ and ω_k, as follows:

$$\min_{\mathbf{u}_k \,\&\, \omega_k} \sum_k \left\| \partial_t \left(\delta(t) + \frac{j}{\pi t} * \mathbf{u}_k(t) \right) \times e^{-j\omega_k t} \right\|_2^2, \; s.t.\ \mathbf{f}(t) = \sum_k \mathbf{u}_k(t) \tag{5}$$

where the sum of the obtained IMFs construct the original signal minus some noise depending on the settings.

The following alternative Lagrangian is constructed to solve the optimisation problem of (5), [32]:

$$\mathcal{L}(\mathbf{u}_k, \omega_k, \lambda) = \alpha \sum_k \left\| \partial_t \left(\delta(t) + \frac{j}{\pi t} * \mathbf{u}_k(t) \right) \times e^{-j\omega_k t} \right\|_2^2 + \left\| \mathbf{f}(t) - \sum_k \mathbf{u}_k(t) \right\|_2^2 + \left\langle \lambda(t), \mathbf{f}(t) - \sum_k \mathbf{u}_k(t) \right\rangle \tag{6}$$

This makes the VMD a parametric decomposition algorithm, requiring its parameters to be specified in computer program settings before running the decomposition algorithm [33]. In this study, the parameters of the VMD and the values selected for each one are listed in Table 1. For further details about how to specify the parameters, the readers are referred to [29]. Three decompositions were selected based on the results of [29].

Seven types of features were selected for each IMF as follows:

1. The centre frequency of the IMF (ω).
2. The Root Mean Square (RMS) of the IF signal obtained for the IMF as follows [29]:

$$\mathrm{RMS_{IF}} = \sqrt{\frac{\sum_{i=1}^{n} \omega(t)^2}{n}}, \tag{7}$$

where $\mathrm{RMS_{IF}}$ is the root mean square of the IF signal $\omega(t)$, and n is the length of the signal.

3. The first quartile of the IF signal, shown as $Q1_{\mathrm{IF}}$, indicates the value under which 25% of IF points are located when they are arranged in ascending order.
4. The second quartile of the IF signal or the median, shown as $Q2_{\mathrm{IF}}$, indicates the value under which 50% of IF points are located when arranged in ascending order.
5. The third quartile of the IF signal, shown as $Q3_{\mathrm{IF}}$, indicates the value under which 75% of IF points are located when arranged in ascending order.

Table 2: The description of all features naming.

Features	Description	Features	Description
x_1	ω of IMF_1	x_{12}	$Q1_{\mathrm{IF}}$ of IMF_2
x_2	$\mathrm{RMS}_{\mathrm{IF}}$ of IMF_1	x_{13}	$Q2_{\mathrm{IF}}$ of IMF_2
x_3	ω of IMF_2	x_{14}	$Q3_{\mathrm{IF}}$ of IMF_2
x_4	$\mathrm{RMS}_{\mathrm{IF}}$ of IMF_2	x_{15}	k_{IF} of IMF_2
x_5	ω of IMF_3	x_{16}	σ_{IF} of IMF_2
x_6	$\mathrm{RMS}_{\mathrm{IF}}$ of IMF_3	x_{17}	$Q1_{\mathrm{IF}}$ of IMF_3
x_7	$Q1_{\mathrm{IF}}$ of IMF_1	x_{18}	$Q2_{\mathrm{IF}}$ of IMF_3
x_8	$Q2_{\mathrm{IF}}$ of IMF_1	x_{19}	$Q3_{\mathrm{IF}}$ of IMF_3
x_9	$Q3_{\mathrm{IF}}$ of IMF_1	x_{20}	k_{IF} of IMF_3
x_{10}	k_{IF} of IMF_1	x_{21}	σ_{IF} of IMF_3
x_{11}	σ_{IF} of IMF_1	–	–

6. The variance of the IF signal, shown as σ_{IF}.
7. The Kurtosis of the IF signal, shown as k_{IF}.

Therefore, there are totally 21 features derived for each test result, named from x_1 to x_{21} as shown in Table 2.

2.2. Feature selection

It is essential to select the most practical features for training the MLAs in order to, first, avoid using uncorrelated features that will only increase the time of the training process, and secondly, prevent overfitting of the model on the training dataset, which will consequently increase the variance between the test set and training set accuracy. To this end, principal component analysis (PCA) is employed to explore the importance of each feature. Generally, the most important features are more correlated with lower order PCs, i.e. PC_1 and PC_2, and components that are not correlated with the lower order PCs are less critical in describing the variability of the dataset across different observations.

Consider the standardised[1] feature matrix $\mathbf{X}_{m\times p}$ of rank $r \leq \min\{m, p\}$, that has the obtained features per observation stacked up in its rows. The singular value decomposition of $\mathbf{X}$ is written as follows:

$$\mathbf{X} = \mathbf{P}\Delta\mathbf{Q}^{\mathrm{T}}, \tag{8}$$

where $\mathbf{P}_{m\times r}$ and $\mathbf{Q}_{p\times r}$ are matrices of left singular and right singular vectors, respectively. Note that $\mathbf{Q}$ is a unitary matrix, i.e. $\mathbf{Q}^{-1} = \mathbf{Q}^{\mathrm{T}}$. Finally, the diagonal matrix of singular values is obtained as $\Delta_{r\times r}$.

[1]The standardised matrix $\mathbf{X}$ is obtained through centring each of its columns concerning the mean value of all the observations in that column divided by their standard deviation.

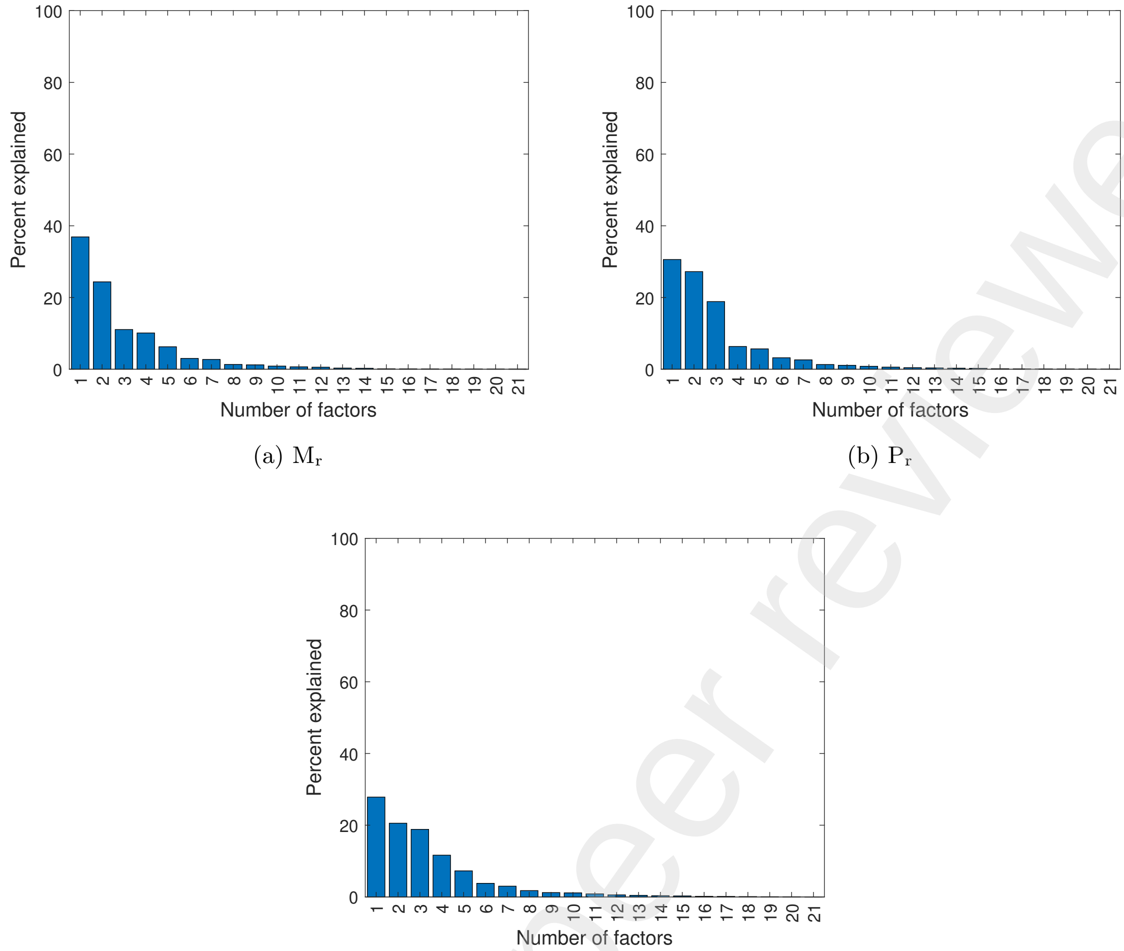

(a) $\mathrm{M_r}$ (b) $\mathrm{P_r}$ (c) Mixed

Figure 1: Scree plots of the PCA applied to the dataset corresponding to the (a) $\mathrm{M_r}$, (b) $\mathrm{P_r}$, (c) mixed observations.

The principal components of $\mathbf{X}$ are stacked up in the columns of the matrix of factor scores, $\mathbf{F}$, obtained as follows:

$$\mathbf{F} = \mathbf{P}\Delta\,, \tag{9}$$

whose columns represent the projected observations on the principal axes. Since $\mathbf{Q}$ is a unitary matrix, one can write:

$$\mathbf{F} = \mathbf{P}\Delta = \mathbf{P}\Delta\mathbf{Q}^{\mathrm{T}}\mathbf{Q} = \mathbf{X}\,\mathbf{Q}\,. \tag{10}$$

Therefore, $\mathbf{Q}$ can also be interpreted as a projection matrix. As such, the contribution of a component to a variable called "loading" is obtained from the calculation of the squared entries of $\mathbf{Q}$. Hence, the rows of $\mathbf{Q}^2$ correspond to the loading of variables evaluated at the principal direction of each column. In order to select the most compelling features for classification, we propose the following procedure to be followed:

1. Obtain the variance percentage explained by each PC corresponding to the standardized feature matrix X.
2. Multiply the variance percentage of the PC to the corresponding column of the $\mathbf{Q}^2$.

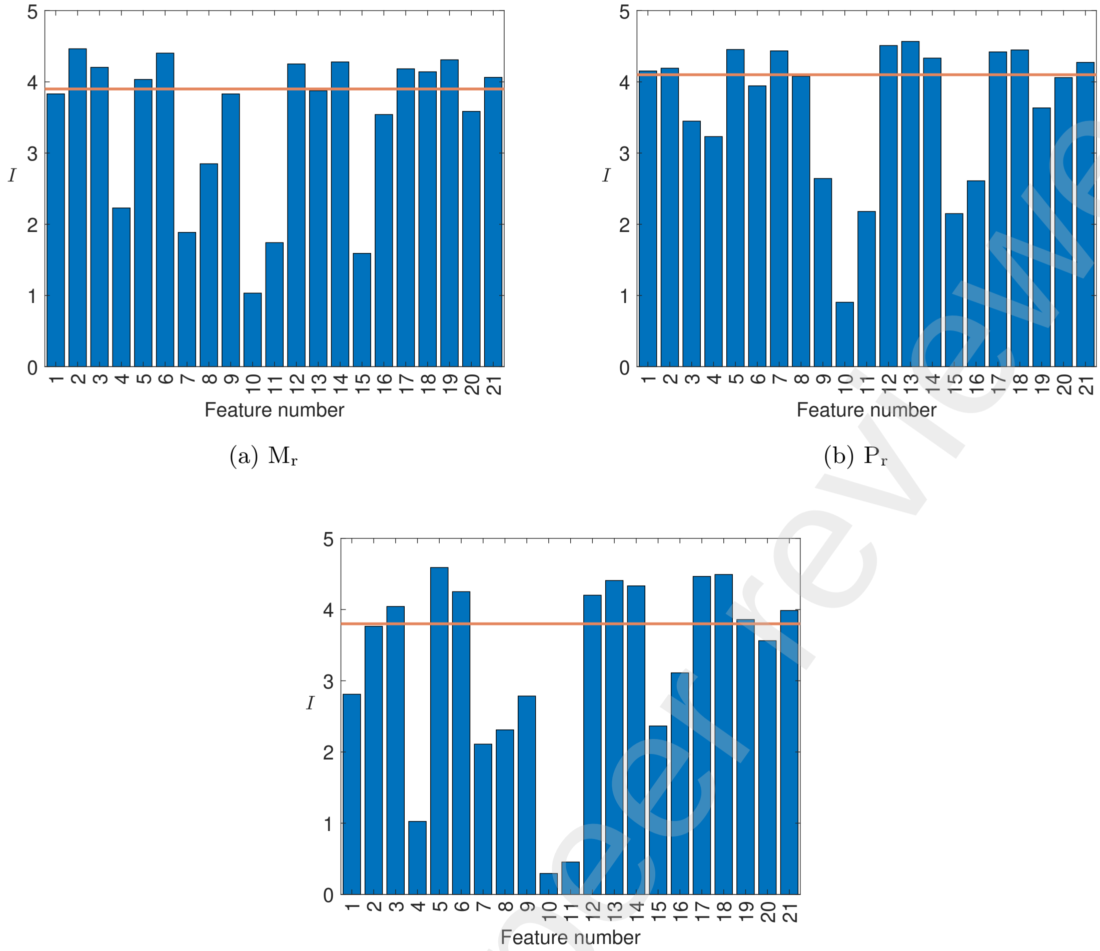

(a) $\mathrm{M_r}$ (b) $\mathrm{P_r}$ (c) Mixed

Figure 2: Contribution percentage of each feature to the first principal dimension for (a) $\mathrm{M_r}$, (b) $\mathrm{P_r}$, (c) mixed observations.

3. Sum the results of step (2) over the selected PCs. Note that one may choose to determine the number of PCs based on the accumulated variance explained by them. However, the first three PCs were selected in this study in all cases.

The above concept can be written in the form of an equation as follows:

$$\mathbf{I} = \sum_{i=1}^{N} var(i) \times \mathbf{Q}^2(:, i) \tag{11}$$

where $\mathbf{I}$ is a vector of obtained importance value for each feature, N is the number of selected PCs, $var(i)$ represents the amount of variance explained by the i^{th} PC, and $N = 3$.

2.3. Employed machine learning algorithms

The machine learning toolbox in MATLAB was exploited to solve the classification problems of this study. The MLAs employed for solving the classification problems are listed in Table 3.

Table 3: MLAs employed for solving the classification problems.

Trees	**Discriminant**	**Naive Bayes**	**SVM**	**Nearest Neighbor**	**Ensemble**
Fine	Linear	Gaussian	Linear	Fine	Boosted Trees
Medium	Quadratic	Kernel	Quadratic	Medium	Bagged Trees
Coarse	–	–	Cubic	Coarse	Subspace Discriminant
–	–	–	Fine Gaussian	Cosine	Subspace KNN
–	–	–	Medium Gaussian	Cubic	RUSBoosted Trees
–	–	–	Coarse Gaussian	Weighted	–

Table 4: Technical specifications of the test set-up.

Ultrasonic device	Pundit PL200
Prob frequency	54 kHz
Sampling frequency	10 MHz
Couplant gel	Proceq Ultraschall-Koppelpaste

3. Lab trial results

In this section, the problem of wood hole-defect classification in two types of wood, i.e. Merbau (hardwood) and Pine (softwood), is solved. The problem of this section is particularly set to serve as a controlled lab trial for classifying wood with natural imperfections in the field. However, similar application can be found in other works such as [34]. The specifications of the test set-up are listed in Table 4. The dimension of the specimens was $90 \times 90 \times 300$ mm^3. There were two types of defects implemented on the specimens: (1) a small hole with a diameter of 6 mm (7% of the cross-section) and (2) a larger hole with a diameter of 13 mm (14% of the cross-section). The hole damage was drilled into the cross-sections. For further details, the readers are referred to [35, 29].

The contact–ultrasonic testing is sensitive to the following items:

1. The amount of the coupling gel applied to the surface of the wood at the transducer and receiver sides.
2. Any vibration of the hands upon testing while holding the transducer and receiver.
3. The amount of pressure applied to the transducer and receiver.

Therefore, 50 replicates of the ultrasonic tests were conducted on each specimen. Table 5 shows the number of tests performed on the samples' different types and health conditions.

Two classes were considered in this study: (1) healthy and (2) defective. As such, small and large damage is classified as defective. This is mainly because the size of the defect is not a matter in standing tree inspection. Therefore, this was done primarily to align with the field trials section. The MLAs listed in Table 3 have been used to answer the following questions:

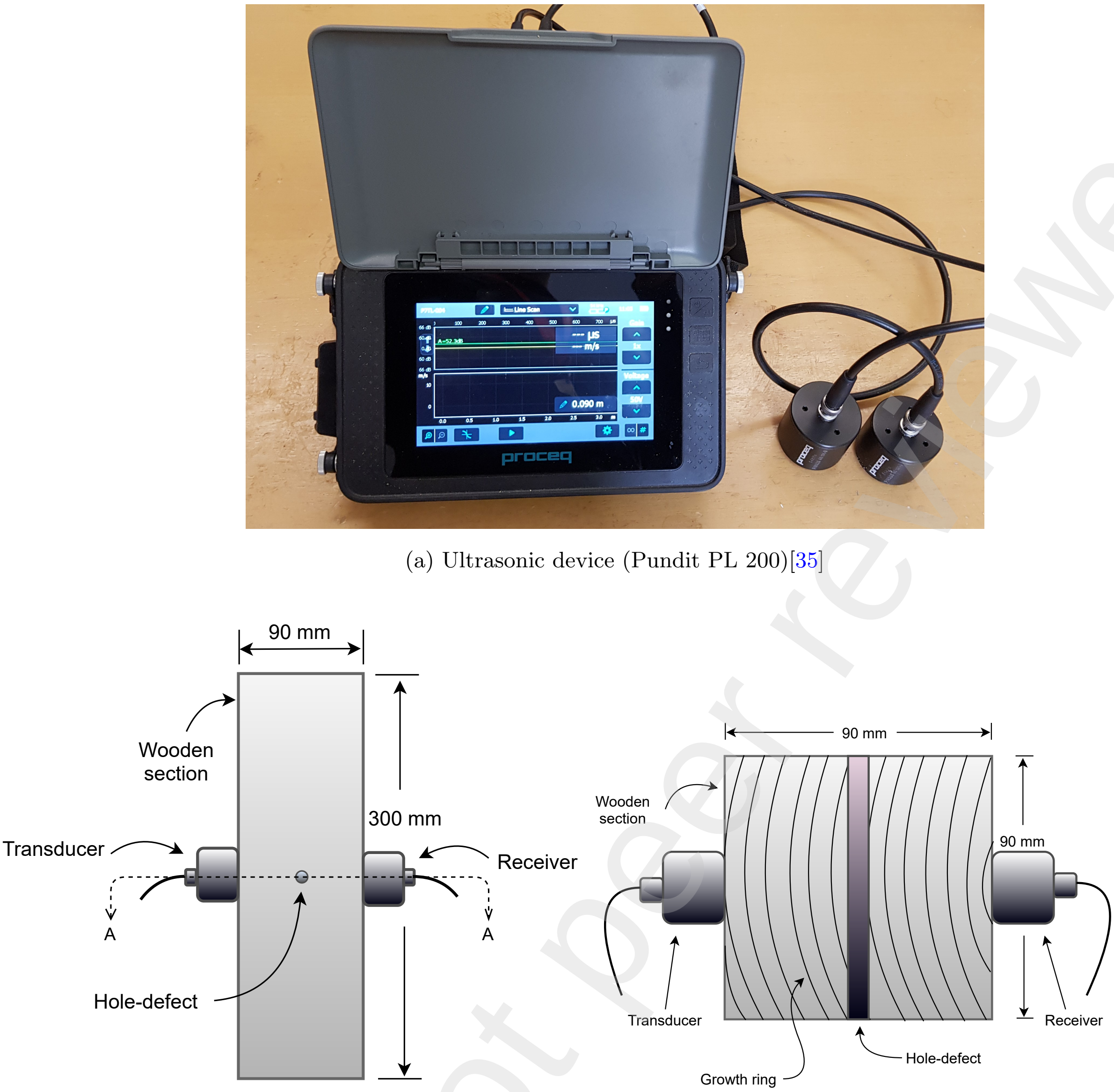

(a) Ultrasonic device (Pundit PL 200)[35]

(b) Schematic of the ultrasonic test

(c) Radial test (A-A)

Figure 3: Ultrasonic test experimental set-up.

1. Do the selected features capture enough variability in the obtained ultrasonic signals across different specimens?
2. How will the trained MLAs perform on a mixture of different types of wood?

Figure 1 shows the scree plots of different types of specimens and a mixture of them. It can be seen that the amount of variance explained by the higher order PCs is always smaller than those described by lower order PCs. Therefore, it is reasonable to select only three first columns of the $\mathbf{Q}^2$ corresponding to the first three PCs in (11). As such, the plots of Figure 2 are obtained that describe the contribution of each feature to the variability of the feature space across different observations, when the observations from different types of wood are considered individually or mixed.

A threshold was set for the value of entries of vector $\mathbf{I}$ for each case to select the first ten most effective features for training. Table 6 shows the selected features for different types of wood based on

Table 5: The number of test samples collected from different types of wood through ultrasonic tests.

Radial test (tangential defect)			
Defect type	**Specimens #**	**Pine test #**	**Merbau test #**
Intact	6	300	300
Small tangential defect	3	150	150
Large tangential defect	3	150	150

Table 6: VMD PARAMETERS.

Type of wood	Selected features
M_r	$x_{21}, x_{19}, x_{18}, x_{17}, x_{14}, x_{12}, x_6, x_5, x_3, x_2$
P_r	$x_{21}, x_{18}, x_{17}, x_{14}, x_{13}, x_{12}, x_7, x_5, x_2, x_1$
Mixture	$x_{21}, x_{19}, x_{18}, x_{17}, x_{14}, x_{13}, x_{12}, x_6, x_5, x_3$

their correlation with the first three PCs. As can be seen from the table, features $x_{21}, x_{18}, x_{17}, x_{14}, x_{12}$, and x_5 are recognised the most effective in all the cases.

Table 7 shows the 5-fold cross-validation accuracy results obtained from the MLA training on each type of wood and their mixture. The results indicate that the "Fine Gaussian SVM" is the most effective algorithm for the classification of all the three problems, i.e. $\mathrm{M_r}$, $\mathrm{P_r}$, and their mixture with the accuracy index of 100, 100, and 99.9 per cent, respectively. The other observation is that the accuracy slightly declines in most cases of using different MLAs when the samples are mixed.

4. Field experimental results

4.1. Using machine learning

In this section, the problem of classification of standing trees based on knot-defect in their trunk is studied. This problem has been given much attention due to its importance in facilitating the mechanised harvesting process. If trees with natural imperfections are appropriately identified, they will not be subject to sawing. This is vital as the bulk of the timber with natural defects is usually sold as pulpwood.

Multiple specimens from different types of wood at various sites in Western Australia (WA) and New South Wales (NSW) were tested using the Pundit PL-200 ultrasonic device. Table 8 shows the types of wood and the environmental conditions at each site upon which the tests were conducted. As such, there was one type of wood (Jarrah) tested in the WA site (Collie) and two different types of wood, namely Blackbutt and Greygum, tested in the NSW site (Coffs harbour). All of these spices, however, are categorised as members of the Eucalyptus family. The temperature in WA and NSW sites was respectively 5.1 and 10 degrees Celsius, while the humidity in both areas was almost equal to 90%. Previous experiences indicate that knot defects appear at the minimum breast height of a standing tree. Therefore, some billets between the breast height and the highest commercial elevation of the

Table 7: The classification results of different MLAs applied to the lab test results.

MLA	M_r	P_r	Mixed
Fine trees	98.5	100	97.8
Medium trees	98.5	100	97.8
Coarse Trees	97.8	100	89.1
Linear Discriminant	97.5	100	86.1
Quadratic Discriminant	100	100	88.8
Gaussian Naïve Byes	81.8	98.7	80.3
Kernel Naïve Byes	95.3	100	84.4
Linear SVM	100	100	87.5
Quadratic SVM	100	100	97.9
Cubic SVM	100	100	99.4
Fine Gaussian SVM	100	100	99.9
Medium Gaussian SVM	100	100	96
Coarse Gaussian SVM	90.2	100	80.4
Fine Nearest Neighbor	100	100	99.8
Medium Nearest Neighbor	100	100	99.6
Coarse Nearest Neighbor	87.7	96.2	82.9
Cosine Nearest Neighbor	100	100	99.3
Cubic Nearest Neighbor	100	100	99.5
Weighted Nearest Neighbor	100	100	99.8
Boosted Trees	50	50	50
Bagged Trees	99.8	100	99.3
Subspace Discriminant	92.5	100	81
Subspace KNN	100	100	99.8
RUSBoosted Trees	50	50	50

corresponding standing trees were harvested and further tested. The breast height was roughly 1.3 m above the highest point of the ground at the base of the tree. The length of the billets was 20 cm each.

Table 9 shows the number of billets from each site and the overall number of ultrasonic tests conducted on them. Likewise, in the lab trial section, there were two labels assigned to the tested specimens, namely healthy and defective, which were specified through visual inspection. The woods were tested through different randomly-selected directions based on how flat the surface of the tested tree was. All specimens were debarked at the point of testing using a hammer. The billets were harvested from 6 standing trees of each species. All trees were visually inspected and marked with a spray marker, as shown in Figure 4.

Table 8: Wood from different sites with different meteorological condition were tested.

State	**Site**	**Wood species**	**Temperature (°C)**	**Humidity (%)**
WA	Collie	Jarrah	5.1	90
NSW	Coffs harbour	Blackbutt & Greygum	10	90

Table 9: The number of billets and ultrasonic tests conducted on woods of different sites.

Number of billets		
Condition	**WA #**	**NSW #**
Intact	37	7
Defective	37	28
Number of ultrasonic test		
Condition	**WA #**	**NSW #**
Intact	838	213
Defective	897	617

The obtained ultrasonic test results were preprocessed using the VMD algorithm to derive the required features, as discussed in Section 2.1. The scree plot of the PCA algorithm applied to the standardized X was first obtained, as shown in Figure 5, to select the most compelling features for training. Then, the variance explained by the first three PCs was used to obtain the effectiveness of features through (11). The contribution of features in the variability of the dataset pertaining to the specimens tested in WA, NSW, and their mixture is presented in Figure 6. Next, a threshold was set for each case to select the ten most useful features, as listed in Table 10. As can be seen from the table, features $x_{21}, x_{18}, x_{17}, x_{13}, x_{12}, x_7, x_4$, and x_2 were identically selected among the most effective features in all cases. This also has an overlap with the most effective features selected for the lab trial cases, which are x_{21}, x_{18}, x_{17} and x_{12}.

Next, the MLAs of Table 3 were employed to solve the classification problem of billets based on their health state in different states. Interestingly, similar to the lab trial results, the Fine Gaussian SVM performs best on all cases of WA, NSW, and a mixture of them with a 5-fold cross-validation accuracy of 93.9, 96.7, and 94 per cent, respectively.

4.2. Using deep learning

Thus far, the results of applying conventional MLAs for solving the classification problem of billets were presented and discussed. However, deep learning architectures have been widely used to solve problems in different fields. Different architectures of deep convolutional neural networks can be found in [36]. In this section, a one-dimensional Convolutional Neural Network (1D-CNN) is developed that takes the identified practical features from the previous sections as input and outputs the class of billets

Figure 4: All trees were visually inspected and marked with spray marker.

as healthy or defective. The architecture of the employed 1D-CNN is depicted in Figure 7. Some essential parameters in the employed 1D-CNN are as follows: learning rate was initially set at 0.01 and was assigned to drop at every 200 epochs with the dropping rate of 0.5; momentum was 0.9; mini-batch size was set at 128; the total epoch number was set at 1000. The damage identification results of these 1D-CNN are presented in Table 12. Table 12 shows the results of the 5-fold cross-validation accuracy for the training and test sets. The results indicate the better performance of the trained 1D-CNN model on billets harvested from NSW sites. This is ideally in line with the results obtained through the machine learning algorithms. Next, the trained models are further tested on some data collected from testing some standing trees.

5. Further testing the trained models

Thus far, the results of solving the classification problem of billets have been presented and discussed. To further assess the capability of the trained models in identifying defective and healthy trees, some trees were tested in WA, from which ten were flawed and nine were healthy. The health state of the trees was determined after cutting down and visual inspection. However, the trees were tested before cutting

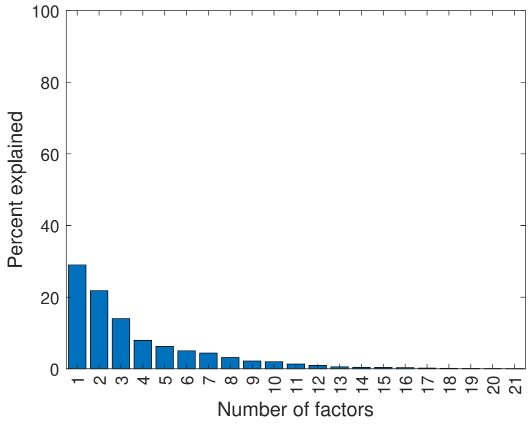

(a) WA

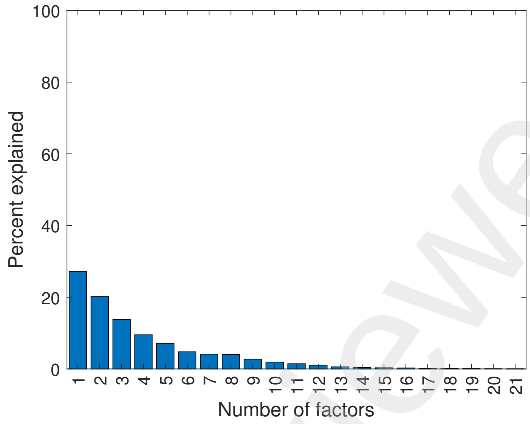

(b) NSW

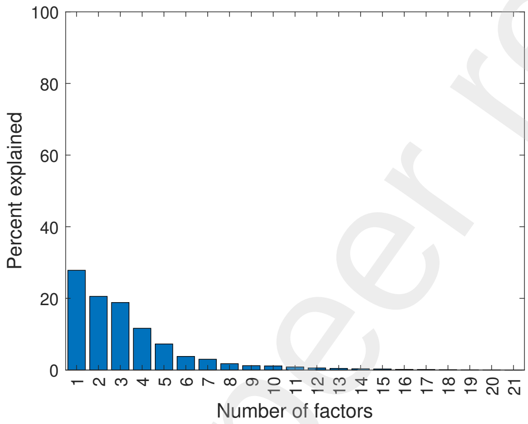

(c) Mixed

Figure 5: Scree plots of the PCA applied to the dataset corresponding to the (a) WA, (b) NSW, (c) mixed observations.

down, and there were 822 ultrasonic signals collected from the sampled trees at their breast height. The optimal MLAs, i.e. Fine Gaussian SVM and the 1D-CNN models trained on the billets harvested from WA, NSW, and a mixture of them, were employed to estimate the health condition of the tested trees. The final accuracy results are reported in Table 13. It was generally expected to achieve poor accuracy when applying the trained models on NSW species for estimating the labels of the tested trees in WA. The results of the table genuinely indicate that this is the case. Moreover, it can be seen from the table results that the Fine Gaussian SVM model trained on the WA billets provides the best accuracy of 87.4%, followed by the 1D-CNN trained on WA billets at 85.5%. However, the accuracy obtained from the 1D-CNN trained on the mixture of billets was 83 %–more than the Fine Gaussian SVM at 78.4%. Interestingly, the 1D-CNN model trained on the NSW performs relatively well when tested on WA trees with an accuracy of 70.1%. The poorest results was obtained from the Fine Gaussian model trained on NSW billets with 58.9% accuracy.

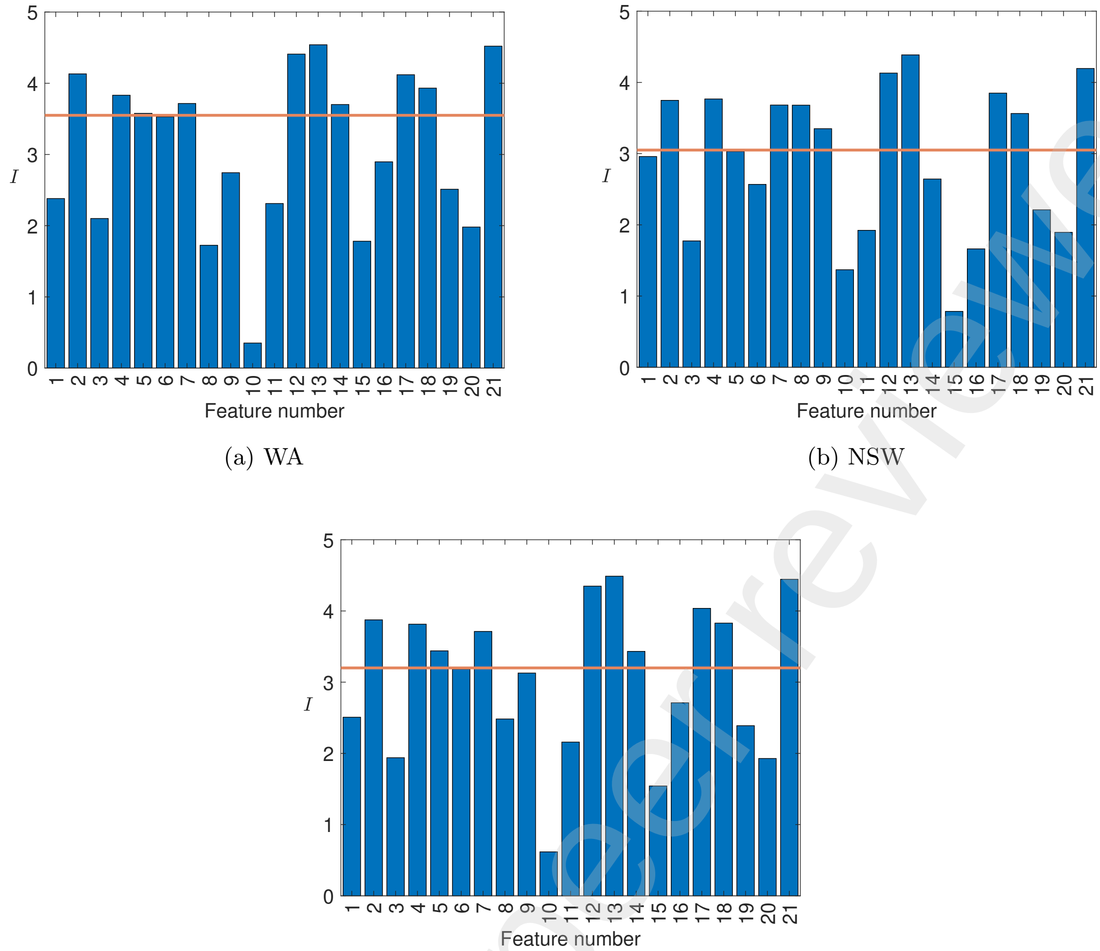

(a) WA

(b) NSW

(c) Mixed

Figure 6: Contribution percentage of each feature to the first principal dimension for (a) WA, (b) NSW, (c) mixed observations.

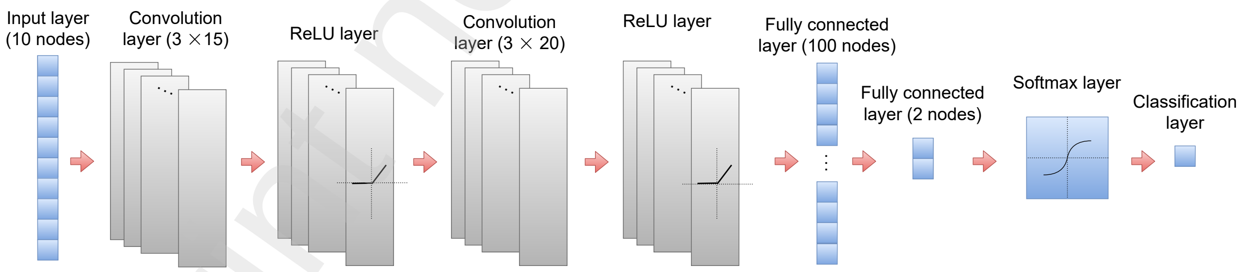

Figure 7: The architecture of the constructed 1D-CNN.

6. Future work

In Section 5, the developed models were further tested on some standing trees. However, the presented accuracy results were not intended for decision-making about accepting or rejecting this null hypothesis that a tested tree is healthy. This is mainly due to the fact that it is not clear how to decide for a tree whose, for instance, more than 50% test outcomes are negative, but still a few positive. Some internal

Table 10: Selected features for each type of wood in different states and a mixture of them.

Type of wood	**Selected features**
WA	$x_{21}, x_{18}, x_{17}, x_{14}, x_{13}, x_{12}, x_7, x_5, x_4, x_2$
NSW	$x_{21}, x_{18}, x_{17}, x_{13}, x_{12}, x_9, x_8, x_7, x_4, x_2$
Mixture	$x_{21}, x_{18}, x_{17}, x_{14}, x_{13}, x_{12}, x_7, x_5, x_4, x_2$

Table 11: The classification results of different MLAs applied to the field test results.

MLA	**WA**	**NSW**	**Mixed**
Fine trees	91.2	94.1	90.3
Medium trees	91.0	94.5	89.8
Coarse Trees	88.2	90.6	85.2
Linear Discriminant	88.0	90.1	85.7
Quadratic Discriminant	87.5	91.3	85.7
Gaussian Naïve Byes	85.4	84.5	82.2
Kernel Naïve Byes	87.5	86.7	85.3
Linear SVM	90.4	91.9	86.8
Quadratic SVM	93.2	95.4	91.6
Cubic SVM	91.8	95.4	92.2
Fine Gaussian SVM	93.9	96.7	94
Medium Gaussian SVM	93.3	95.2	91.7
Coarse Gaussian SVM	90.4	90.4	87.1
Fine Nearest Neighbor	91.2	94.8	91.5
Medium Nearest Neighbor	93.5	95.3	92.9
Coarse Nearest Neighbor	88.0	87.5	85.7
Cosine Nearest Neighbor	92.2	93.6	91.8
Cubic Nearest Neighbor	93.5	94.9	92.8
Weighted Nearest Neighbor	93.3	95.9	94.1
Boosted Trees	92.7	94.9	92
Bagged Trees	93.3	96.4	93.3
Subspace Discriminant	86.6	90.1	85.2
Subspace KNN	91.5	96.5	92.2
RUSBoosted Trees	91.9	95.5	90.7

defects in the wooden sections may not be deemed as significant defects and may not thus exclude the tree from being used for industrial purposes. For such defects, it is evident that the test result obtained from testing through some particular angles may be positive. This is schematically demonstrated in

Table 12: The 5-fold cross validation accuracy results obtained for the training and test sets using the trained 1D-CNN models.

Accuracy	**WA**	**NSW**	**Mixed**
Training	96.3	99.7	97.8
Testing	92.5	96.3	92.2

Table 13: The training and testing accuracy of the trained CNN models.

Model	**CNN**	**Fine Gaussian SVM**
WA	83.1	87.4
Mixed	84.5	78.4
NSW	66.8	58.9

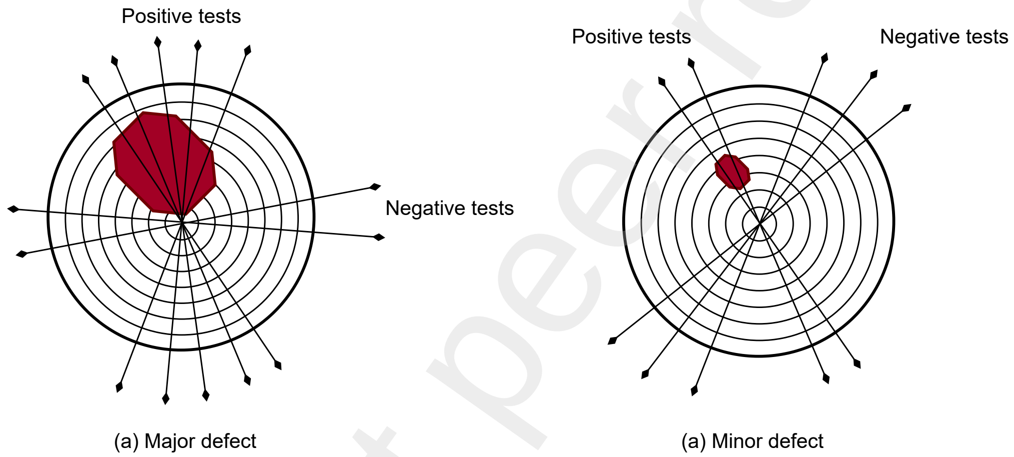

Figure 8: Testing a cross section of a tree with (a) major defect, and (b) minor defect.

Figure 8. Therefore, further works need to be done on the decision-making part of the proposed strategy to make assigning a label to a tested tree more rational for practical applications. This is indeed the subject of future work.

7. Conclusions

The problem of mechanized harvesting of standing trees has been targeted through solving the classification problem of trees using contact–ultrasonic testing and machine learning algorithm. To this end, the contact–ultrasonic test results were first decomposed into their constituent components using the VMD algorithm to derive some features. The importance of each feature was then identified through a new equation based on the loading of each feature corresponding to a PC and the amount of variance explained by that PC summed over all the first three PCs, obtained from the PCA analysis of the standardized feature matrix. Several test results were obtained from lab specimens, and sites of the two states in Australia, i.e. WA and NSW, were studied. The results of the lab trial were interestingly well aligned with those obtained from the fields. For instance, the Fine Gaussian SVM was proven to be the most effective MLA for solving the classification problem in both cases. Moreover, it was shown that in both cases features x_{21}, x_{18}, x_{17}, and x_{12} were among the most effective features for solving the classification problem. These features correspond respectively to the σ_{IF} of IMF_3, $Q2_{IF}$ of IMF_3, $Q1_{IF}$ of IMF_3, and $Q1_{IF}$ of IMF_2.

A 1D-CNN model was also established for solving the classification problem of billets obtained from the trees harvested in the fields. The results indicate that both the Fine Gaussian algorithm and 1D-CNN can effectively solve the classification problems of wood classifications in the fields, where at worst 92.4% classification accuracy was obtained for the mixture of the billets obtained from WA and NSW sites.

The trained models were then employed to predict the health label of some defective standing trees in WA sites. The results indicated that accuracy above 85% was achieved when models trained on the WA billets were employed. Nevertheless, this accuracy declined as the models trained on a mixture of billets from different cites (and, therefore, different types of wood) were employed. As such, the accuracy obtained from the 1D-CNN was still at an acceptable level of 83%, while the accuracy index obtained from the Fine Gaussian SVM plunged to 78.4%. Further, the models trained on the NSW billets were employed to predict the label of the standing trees in WA. Although expected that the results would plunge drastically, the 1D-CNN results were surprisingly at an acceptable level of 70.1%. However, the accuracy index obtained from the Fine Gaussian algorithm was at 58.9%, which is not near the one obtained from the 1D-CANN algorithm.

Overall, the results of this study pave the way for solving the classification problem of the standing trees based on their health condition. This paper's results also confirm the effectiveness of the features obtained from the time-frequency domain of the ultrasonic signals using the VMD algorithm. However, further works need to be done on the decision-making part of the problem, where the test results from different angles on a cross-section of the tree (mainly the breast height) are used to wisely decide whether the tree is actually helpful for industrial purposes.

Acknowledgement

The authors appreciate the support provided by Forest and Wood Products Australia (FWPA), Forestry Corporation NSW and Forest Products Commission (FPC).

Conflict of interest

On behalf of all authors, the corresponding author states that there is no conflict of interest.

References

[1] A. Abid, M. T. Khan, J. Iqbal, A review on fault detection and diagnosis techniques: basics and beyond, Artificial Intelligence Review 54 (5) (2021) 3639–3664.

[2] C. L. Goh, R. A. Rahim, M. H. F. Rahiman, M. T. M. Talib, Z. C. Tee, Sensing wood decay in standing trees: A review, Sensors and Actuators A: Physical 269 (2018) 276–282.

[3] T. Palander, J. Eronen, K. Kärhä, H. Ovaskainen, Development of a wood damage monitoring system for mechanized harvesting, Annals of Forest Research 61 (2) (2018) 243–258.

[4] S.-J. Pang, K.-B. Shim, K.-H. Kim, Effects of knot area ratio on the bending properties of cross-laminated timber made from korean pine, Wood Science and Technology 55 (2) (2021) 489–503.

[5] H. Yang, L. Yu, Feature extraction of wood-hole defects using wavelet-based ultrasonic testing, Journal of forestry research 28 (2) (2017) 395–402.

[6] G. López, L. A. Basterra, L. Acuña, Estimation of wood density using infrared thermography, Construction and Building Materials 42 (2013) 29–32.

[7] W. Li, J. Van den Bulcke, D. Mannes, E. Lehmann, I. De Windt, M. Dierick, J. Van Acker, Impact of internal structure on water-resistance of plywood studied using neutron radiography and X-ray tomography, Construction and Building Materials 73 (2014) 171–179.

[8] E. Blomme, D. Bulcaen, F. Declercq, Air-coupled ultrasonic nde: experiments in the frequency range 750 kHz–2 MHz, NDT & E International 35 (7) (2002) 417–426.

[9] A. C. Senalik, G. Schueneman, R. J. Ross, Ultrasonic-based nondestructive evaluation methods for wood: a primer and historical review, USDA Forest Service, Forest Products Laboratory, General Technical Report, FPL-GTR-235, 2014; 36 p. 235 (2014) 1–36.

[10] T. Goto, Y. Tomikawa, S. Nakayama, T. Furuno, Changes of propagation velocity of ultrasonic waves and partial compression strength of decay-treated woods relationship between decrease of propagation velocity of ultrasonic waves and remaining strength, Mokuzai Gakkaishi 57 (6) (2011) 359–369.

[11] S. Lee, S.-J. Lee, J. S. Lee, K.-B. Kim, J.-J. Lee, H. Yeo, Basic study on nondestructive evaluation of artificial deterioration of a wooden rafter by ultrasonic measurement, Journal of Wood Science 57 (5) (2011) 387–394.

[12] F. Tallavo, G. Cascante, M. D. Pandey, A novel methodology for condition assessment of wood poles using ultrasonic testing, NDT & E International 52 (2012) 149–156.

[13] T. Mori, Y. Yanase, K. Tanaka, K. Kawano, Y. Noda, M. Mori, H. Kurisaki, K. Komatsu, Evaluation of compression and bending strength properties of wood damaged from bio-deterioration, Journal of the Society of Materials Science, Japan 62 (4) (2013) 280–285.

[14] S.-J. Lee, S. Lee, S.-J. Pang, C.-K. Kim, K.-M. Kim, K.-B. Kim, J.-J. Lee, Indirect detection of internal defects in wooden rafter with ultrasound, Journal of the Korean Wood Science and Technology 41 (2) (2013) 164–172.

[15] A. Ettelaei, M. Layeghi, H. Z. Hosseinabadi, G. Ebrahimi, Prediction of modulus of elasticity of poplar wood using ultrasonic technique by applying empirical correction factors, Measurement 135 (2019) 392–399.

[16] S. Lee, S.-J. Lee, J. S. Lee, K.-B. Kim, J.-J. Lee, H. Yeo, Basic study on nondestructive evaluation of artificial deterioration of a wooden rafter by ultrasonic measurement, Journal of wood science 57 (5) (2011) 387–394.

[17] L. Reinprecht, M. Pánek, Ultrasonic technique for evaluation of bio-defects in wood: Part 1–influence of the position, extent and degree of internal artificial rots, International Wood Products Journal 3 (2) (2012) 107–115.

[18] M. Mori, M. Hasegawa, J.-C. Yoo, S.-G. Kang, J. Matsumura, Nondestructive evaluation of bending strength of wood with artificial holes by employing air-coupled ultrasonics, Construction and Building Materials 110 (2016) 24–31.

[19] C.-J. Lin, Y.-C. Kao, T.-T. Lin, M.-J. Tsai, S.-Y. Wang, L.-D. Lin, Y.-N. Wang, M.-H. Chan, Application of an ultrasonic tomographic technique for detecting defects in standing trees, International Biodeterioration & Biodegradation 62 (4) (2008) 434–441.

[20] L. Krajnc, A. Kadunc, A. Straže, The use of ultrasound velocity and damping for the detection of internal structural defects in standing trees of european beech and norway spruce, Holzforschung 73 (9) (2019) 807–816.

[21] L. Espinosa, J. Bacca, F. Prieto, P. Lasaygues, L. Brancheriau, Accuracy on the time-of-flight estimation for ultrasonic waves applied to non-destructive evaluation of standing trees: a comparative experimental study, Acta Acustica united with Acustica 104 (3) (2018) 429–439.

[22] L. Drain, Laser ultrasonics techniques and applications, Routledge, 2019.

[23] M. Hirao, H. Ogi, EMATs for science and industry: noncontacting ultrasonic measurements, Springer Science & Business Media, 2013.

[24] W. Grandia, C. Fortunko, Nde applications of air-coupled ultrasonic transducers, in: 1995 IEEE Ultrasonics Symposium. Proceedings. An International Symposium, Vol. 1, IEEE, 1995, pp. 697–709.

[25] Y. Fang, L. Lin, H. Feng, Z. Lu, G. W. Emms, Review of the use of air-coupled ultrasonic technologies for nondestructive testing of wood and wood products, Computers and electronics in agriculture 137 (2017) 79–87.

[26] D. Chimenti, Review of air-coupled ultrasonic materials characterization, Ultrasonics 54 (7) (2014) 1804–1816.

[27] T. Marhenke, J. Neuenschwander, R. Furrer, J. Twiefel, J. Hasener, P. Niemz, S. J. Sanabria, Modeling of delamination detection utilizing air-coupled ultrasound in wood-based composites, NDT & E International 99 (2018) 1–12.

[28] M. S. Taskhiri, M. H. Hafezi, R. Harle, D. Williams, T. Kundu, P. Turner, Ultrasonic and thermal testing to non-destructively identify internal defects in plantation eucalypts, Computers and Electronics in Agriculture 173 (2020) 105396.

[29] M. Mousavi, A. H. Gandomi, Wood hole-damage detection and classification via contact ultrasonic testing, Construction and Building Materials 307 (2021) 124999.

[30] D. Gabor, Theory of communication. part 1: The analysis of information, Journal of the Institution of Electrical Engineers-Part III: Radio and Communication Engineering 93 (26) (1946) 429–441.

[31] I. Muskhelishvili, Nikolaĭ, J. R. M. Radok, Singular integral equations: boundary problems of function theory and their application to mathematical physics, Courier Corporation, 2008.

[32] K. Dragomiretskiy, D. Zosso, Variational mode decomposition, IEEE Transactions on Signal Processing 62 (3) (2014) 531–544.

[33] D. Zosso, Variational mode decomposition, matlab central file exchange (Retrieved August 27, 2020).
URL https://www.mathworks.com/matlabcentral/fileexchange/44765-variational-mode-decomposition

[34] A. Jegorowa, J. Kurek, I. Antoniuk, W. Dołowa, M. Bukowski, P. Czarniak, Deep learning methods for drill wear classification based on images of holes drilled in melamine faced chipboard, Wood Science and Technology 55 (1) (2021) 271–293.

[35] M. Mousavi, M. S. Taskhiri, D. Holloway, J. Olivier, P. Turner, Feature extraction of wood-hole defects using empirical mode decomposition of ultrasonic signals, NDT & E International (2020) 102282.

[36] A. Khan, A. Sohail, U. Zahoora, A. S. Qureshi, A survey of the recent architectures of deep convolutional neural networks, Artificial intelligence review 53 (8) (2020) 5455–5516.